Role of denatured-state properties in chaperonin action probed by single-molecule spectroscopy

Hofmann, Hagen ; Hillger, Frank ; Delley, Cyrille ; Hoffmann, Armin ; Pfeil, Shawn H ; Nettels, Daniel ; Lipman, Everett A ; Schuler, Benjamin

Abstract: The bacterial chaperonin GroEL/GroES assists folding of a broad spectrum of denatured and misfolded proteins. Here, we explore the limits of this remarkable promiscuity by mapping two denatured proteins with very different conformational properties, rhodanese and cyclophilin A, during binding and encapsulation by GroEL/GroES with single-molecule spectroscopy, microfluidic mixing, and ensemble kinetics. We find that both proteins bind to GroEL with high affinity in a reaction involving substantial conformational adaptation. However, whereas the compact denatured state of rhodanese is encapsulated efficiently upon addition of GroES and ATP, the more expanded and unstructured denatured cyclophilin A is not encapsulated but is expelled into solution. The origin of this surprising disparity is the weaker interactions of cyclophilin A with a transiently formed GroEL-GroES complex, which may serve as a crucial checkpoint for substrate discrimination.

DOI: https://doi.org/10.1016/j.bpj.2014.11.002

Article

Role of Denatured-State Properties in Chaperonin Action Probed by Single-Molecule Spectroscopy

Hagen Hofmann,[1,*] Frank Hillger,[1] Cyrille Delley,[1] Armin Hoffmann,[1] Shawn H. Pfeil,[2] Daniel Nettels,[1] Everett A. Lipman,[2] and Benjamin Schuler[1,*]

[1]Department of Biochemistry, University of Zurich, Zurich, Switzerland; and [2]Department of Physics, University of California, Santa Barbara, Santa Barbara, CA

ABSTRACT The bacterial chaperonin GroEL/GroES assists folding of a broad spectrum of denatured and misfolded proteins. Here, we explore the limits of this remarkable promiscuity by mapping two denatured proteins with very different conformational properties, rhodanese and cyclophilin A, during binding and encapsulation by GroEL/GroES with single-molecule spectroscopy, microfluidic mixing, and ensemble kinetics. We find that both proteins bind to GroEL with high affinity in a reaction involving substantial conformational adaptation. However, whereas the compact denatured state of rhodanese is encapsulated efficiently upon addition of GroES and ATP, the more expanded and unstructured denatured cyclophilin A is not encapsulated but is expelled into solution. The origin of this surprising disparity is the weaker interactions of cyclophilin A with a transiently formed GroEL-GroES complex, which may serve as a crucial checkpoint for substrate discrimination.

INTRODUCTION

The cellular machinery of molecular chaperones (1–4), quality control systems (3), and components that translocate and degrade proteins reflects the importance of protein homeostasis in the cell. To control protein folding, misfolding, and aggregation, these cellular factors can exert forces that will affect the conformation and dynamics of proteins (4,5). However, the complexity and promiscuity (6–8) of this machinery often complicate detailed mechanistic investigations of the underlying physical principles. For example, it has been suggested that the confinement of proteins inside a cavity, as formed by the heptameric rings of GroEL and GroES (1–4,9), can stabilize proteins (10,11) and accelerate protein folding reactions (12–16). However, results from experiments and simulation also show that this accelerating effect can be countered by interactions of the substrate with the GroEL-GroES cavity wall (12,17–20). To delineate these contributions we need to better understand the effect of GroEL on the conformation and dynamics of denatured proteins. Here, we compare two proteins with very different denatured-state properties, a destabilized variant of human cyclophilin A (CypA) (21–23) and bovine rhodanese (Rho) (24) (Fig. 1 *a*) (25,26). Both proteins are known to bind to GroEL in vitro (23,24,27,28) and are identified as GroEL-binding-competent based on a sequence comparison with 284 GroEL substrates identified in *Escherichia coli* (Fig. 1, *b* and *c*) (6,7,26). Although human CypA and bovine Rho have very similar mean net charge and hydrophobicity (Fig. 1 *b*), the two proteins differ substantially in their length; bovine Rho (296 amino acids (aa)) is almost twice as large as human CypA (167 aa). Of most importance, however, previous experiments indicate that their GroEL-bound states are very different: whereas CypA bound to GroEL was shown to exhibit substantial dynamics with a lack of stable secondary structure (23,29), recent NMR experiments indicate that 85% of the amino acids in Rho are immobile in complex with GroEL (30). Thus, the two proteins represent different parts of the broad substrate spectrum of the promiscuous GroEL/ES chaperone (Fig. 1 *c*). To investigate the conformational properties and dynamics of both proteins along the encapsulation pathway, we employ a combination of single-molecule Förster resonance energy transfer (smFRET), microfluidic mixing, fluorescence correlation spectroscopy, and ensemble kinetic experiments.

MATERIALS AND METHODS

Single-molecule fluorescence spectroscopy

Measurements were performed at 22°C in 50 mM TrisHCl, 10 mM $MgCl_2$, 5 mM KCl, 100 mM 2-mercaptoethanol, 0.001% Tween 20, pH 7.5, using either a custom-built confocal microscope, as described previously (17), or a Micro Time 200 confocal microscope equipped with a HydraHarp 400 counting module (Picoquant, Berlin, Germany). The donor dye was excited with a diode laser at 485 nm (dual mode: continuous wave and

Submitted August 13, 2014, and accepted for publication November 3, 2014.

*Correspondence: hagen.hofmann@weizmann.ac.il or schuler@bioc.uzh.ch

Hagen Hofman's present address is Department of Structural Biology, Weizmann institute of Science, Rehovot 7600, Israel.

Frank Hillger's present address is Novartis Institutes for BioMedical Research, Novartis International AG, 4002 Basel, Switzerland.

Armin Hoffman's present address is Celonic AG, 8051 Basel, Switzerland.

Shawn H. Pfeil's present address is Department of Physics, West Chester University of Pennsylvania, West Chester, PA 19383

Editor: Ashok Deniz.

0006-3495/14/12/2891/12 $2.00

http://dx.doi.org/10.1016/j.bpj.2014.11.002

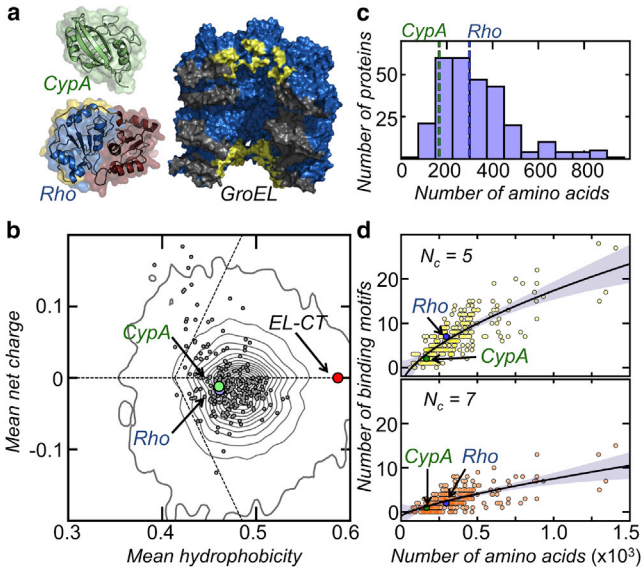

FIGURE 1 Structure and sequence characteristics of Rho and CypA. (*a*) Structure of cyclophilin (CypA; Protein Data Bank (PDB) 1OCA) and rhodanese (Rho; PDB 1RHS), with a surface representation of GroEL in its ADP state (PDB 1XCK). For clarity, four subunits of each ring have been removed. The substrate-binding region in the apical domains is shown in yellow. The size of the structures is not to scale. (*b*) Mean net charge versus mean hydrophobicity for 50,000 amino acid sequences drawn from the natural abundance of amino acids (35) (*contours*), for 284 identified GroEL substrates (*gray circles*) (6,7,18), CypA (*green circle*), Rho (*blue circle*), and the last 17 amino acids of the C-terminal tail of GroEL (*red circle*). (*c*) Sequence length distribution of 284 identified GroEL substrates (6). Dashed lines indicate the lengths of CypA (*green*) and Rho (*blue*). (*d*) Scaling of the number of GroEL binding motifs (18) PXHHH ($N_c = 5$) and PXHHHXP ($N_c = 7$) (P, polar amino acid; H, hydrophobic amino acid; X, any amino acid) with the protein length for 284 identified GroEL substrates from *E. coli* (6,7,18). The solid line is a fit according to $y = a^x + y_0$ and indicates the average of the sequence length distribution of GroEL binding motifs. CypA (*green*) and Rho (*blue*) are close to this average. To see this figure in color, go online.

pulsed; LDH-D-C-485, PicoQuant) at an average power of 200 μW. smFRET efficiency histograms were acquired in samples with a protein concentration of ~20–50 pM, with the laser in continuous-wave mode; photon counts were recorded at a resolution of 16 ps by the counting electronics (time resolution was thus limited by the timing jitter of the detectors). For dual-color excitation, the acceptor was excited in addition to the donor with picosecond pulses at a wavelength range selected by a z582/15 (Chroma, Bellows Falls, VT) band-pass filter and a pulse frequency of 20 MHz (Optical Supercontinuum Systems SCF450-4-20MHz, Fianium, Southampton, United Kingdom). Successive photons detected in either channel and separated by <100 μs were combined in one burst. A burst was retained as a significant event if the total number of counts exceeded 50 for free CypA or CypA-SR1 complexes or 25 for experiments using the microfluidic mixing device. For Rho-SR1 complexes or denatured Rho, a threshold of 20 for Rho-SR1 was used. Identified bursts were corrected for background, differences in quantum yields of donor and acceptor, the different collection efficiencies in the detection channels, cross talk, and direct acceptor excitation, as described previously (31). In addition, bursts during which acceptor photobleaching was likely to have occurred were discarded (27).

The quantum yields of the attached fluorophores are substantially lowered in all denatured Rho variants at 0.4 M guanidinium chloride (GdmCl), indicative of photoinduced electron transfer (PET) between exposed aromatic amino acids and the attached fluorophores (17). However, PET affects $\langle E \rangle$ only via quenching of the acceptor fluorophore, and the observed transfer efficiencies are thus lower bounds for the true values (32). Static quenching (PET) of the donor fluorophore does not affect the transfer efficiencies, because neither the donor nor the acceptor emits photons in this case. In general, uncertainties in observed transfer efficiencies of ~0.03 were estimated from the variations in the experimentally determined correction factor, which takes into account differences in detection efficiencies and quantum yields of the two fluorophores (31) over a period of 3 years.

Microfluidic mixing experiments

For rapid mixing experiments, microfluidic mixers fabricated by replica molding in polydimethylsiloxane were used as described previously (17,33). For experiments using the microfluidic device, the Tween 20 concentration was increased to 0.01% to prevent surface adhesion of the proteins. The transfer efficiency histograms for denatured CypA and Rho at 0.4 M GdmCl were obtained by mixing denatured protein in 4 M GdmCl with buffer at a flow rate of 0.8 mm/s by placing the confocal volume at position 100 μm (125 ms) downstream of the mixing region. The applied pressures were 10.4 kPa (1.5 psi) in the two buffer channels and 6.8 kPa (1 psi) in the sample channel. The kinetics of CypA dissociation from GroEL-SR1 on mixing with ATP and GroES were obtained at a flow rate of 1.2 mm/s with a pressure of 2 psi in all channels.

For detection of the GroES-ATP-mediated release of the SR1-bound CypA variants, the binary CypA-SR1 complex was mixed at a ratio of 1:5.7 with 2.4 mM ATP and varying concentrations of GroES, resulting in final concentrations of 0.5 μM, 1 μM, 1.6 μM, and 3 μM GroES, and 2 mM ATP. The experiments were performed at pressures of 13.8 kPa (2.0 psi) applied to all channels, resulting in a mean velocity of 1.2 mm/s that was used to convert distances to times, as described by Pfeil et al. (33). The calculated velocities were checked by analyzing the donor-acceptor fluorescence intensity cross-correlation functions and the obtained rate constants k_1 and k_2 were corrected for variations in the flow between the different microfluidic chips used for the experiments. To determine the transfer efficiency histogram at $t = 0$, the binary CypA-SR1 complex was measured in the observation channel of the mixing device without ATP and GroES in the buffer channels.

Two-focus fluorescence correlation spectroscopy

Two-focus fluorescence correlation spectroscopy (2f-FCS) measurements (34) were performed at 22°C on a Micro Time 200 confocal microscope (PicoQuant) equipped with a differential interference contrast prism. The donor dye was excited alternatively with two orthogonally polarized diode lasers at 483 nm (LDH-D-C-485, PicoQuant) at a repetition rate of 20 MHz and a laser power of 30 μW each. The distance between the two foci was determined as described previously (35).

Binding isotherms of denatured CypA or carbamidomethylated rhodanese (CAM-Rho) were obtained at a substrate concentration of 0.725 nM for CAM-Rho58 labeled with AlexaFluor 488 and AlexaFluor 594 or 0.125 nM for CypA-V2C-A488, respectively. Before measurement, the samples were incubated at 22°C for 2 h (CypA-SR1) and 12 h (CypA-SR1+ATPγS, Rho-SR1, and RhoSR1-ATPγS). The change in the Stokes radii on addition of GroEL-SR1 were fitted according to

$$R_H = \frac{\Delta R_H}{2P_0}\left(P_0 + [SR1]_0 + K_D - \sqrt{\left(P_0 + K_D + [SR1]_0\right)^2 - 4P_0[SR1]_0}\right) + R_{H0}. \quad (1)$$

Here, ΔR_H is the change in R_H between free and completely bound substrate, P_0 is the total concentration of CypA and Rho, $[SR1]_0$ is the total concentration of GroEL-SR1 and R_{H0} is the Stokes radius in the absence of chaperone.

GroEL-SR1 binding kinetics of CypA and Rho using stopped-flow mixing

The nonlinear dependence of the pseudo-first-order binding rate constant (k) on GroEL-SR1 concentration was described by a kinetic model including the fast formation of a transient encounter complex using

$$k = \frac{k_{max}[SR1]}{K + [SR1]}, \quad (2)$$

where k_{max} is the rate constant for the rate-limiting conformational adaptation to the GroEL-SR1 surface and K is the dissociation constant for the encounter complex. The temperature dependence of K is given by

$$K = \exp\left(\frac{\Delta H_{eq} - T\Delta S_{eq}}{RT}\right), \quad (3)$$

where ΔH_{eq} is the enthalpy change and ΔS_{eq} is the entropy change on formation of the encounter complex relative to free substrate and free GroEL-SR1, R is the ideal gas constant, and T is the temperature. The temperature dependence of k_{max} is given by

$$k_{max} = k_0 \exp\left[-\frac{\Delta H_0^{\ddagger} + \Delta C^{\ddagger}(T - T_0) - T\left(\Delta S_0^{\ddagger} + \Delta C^{\ddagger}\ln(T/T_0)\right)}{RT}\right], \quad (4)$$

with $\Delta H_0^{\ddagger}$ and $\Delta S_0^{\ddagger}$ being the change in activation enthalpy and entropy at $T_0 = 298$ K and $\Delta C^{\ddagger}$ being the change in heat capacity between the encounter complex and the top of the adaptation barrier. The preexponential factor k_0 was given by

$$k_0(T) = \tau_0^{-1}\frac{\eta(T_0)}{\eta(T)} \quad (5\text{-}1)$$

with

$$\eta(T) = \eta_0 \exp\left[\frac{B}{R(T - \theta)}\right], \quad (5\text{-}2)$$

with $\tau_0^{-1} = 10^6\ s^{-1}$ as estimated from the ns-FCS measurements ($\tau_0 = 1\ \mu s$) and $T_0 = 298$ K (see the Supporting Material). Under the assumption that internal friction does not dominate the reaction (36), the temperature dependence of water viscosity was taken into account using the empirical equation (Eq. 5-2) with $\eta_0 = 2.4152\ 10^{-5}$ Pa s, $B = 4.7428$ kJ mol^{-1}, and $\theta = 139.86$ K (37).

Chemical modification of CypA (K28C) labeled with AlexaFluor 488

For cross-linking with Ru^{3+} (38), 2 μM of the CypA variant K28C-A488 was incubated with 1 mM tris-bipyridylruthenium chloride ($Ru(bpy)_3Cl_2$) and 20 mM ammonium persulfate in 40 μL of 50% methanol/water. The sample was illuminated for 2–4 s by a continuous-wave laser at 488 nm with a power of 12 mW. Immediately after illumination, the reaction was quenched by the addition of dithiotreitol to a final concentration of 50 mM. To suppress aggregation, GdmCl was also added to a final concentration of 3 M. The modification of the amino groups of 20 μM of the K28C-A488 variant with 2 mM LC-SPDP (succinimidyl 6-[3′-(2-pyridyldithio)-propionamido] hexonate) was performed for 4 h in 50 mM sodium phosphate, pH 7.0, and 6 M GdmCl at 25°C. The reaction was stopped by the addition of TrisHCl-buffer (pH 7) with a final concentration of 50 mM. Without further purification, the reaction mixtures were diluted to a concentration of 1 nM in 50 mM TrisHCl, 10 mM $MgCl_2$, and 5 mM KCl, pH 7.5, with varying concentrations of GdmCl to obtain the Stokes radii of the two chemically modified CypA-variants. The complexes of the chemically modified CypA variants with GroEl-SR1 were purified with analytical size-exclusion chromatography before measurement.

Calculation of the entropy cost of confinement

The partition function for a Gaussian chain confined inside a cylinder (10) with height h and diameter d is

$$Z_{Chain} = \pi r^2 h\left(\frac{32}{\pi^2}\right)\left[\sum_{k=1,2,3\ldots}\frac{1}{x_k^2}\exp\left(-\frac{x_k^2 l_p N b}{3r^2}\right)\right] \times \left[\sum_{k=1,3,5\ldots}\frac{1}{k^2}\exp\left(-\frac{\pi^2 k^2 l_p N b}{3h^2}\right)\right]. \quad (6)$$

Here, r is the radius of the confining cylinder, h is the height of the cylinder, l_p is the persistence length of the confined chain, N is the number of bonds in the chain, b is the bond length, in our case the distance between two successive Cα-atoms (0.38 nm), and x_k are the roots of $J_0(x)$, the Bessel function of the first kind of order zero ($x_1 = 2.4$, $x_2 = 5.52$, $x_3 = 8.65$,…) (10). The term $\pi r^2 h$ in Eq. 6 accounts for the translational degrees of freedom of the chain. The free energy of the chain (in k_BT) inside a cylinder is given by

$$F_{Chain} = -\ln\left(\frac{Z_{Chain}}{\pi r^2 h}\right). \quad (7)$$

We calculated F_{Chain} for CypA with $N = 166$, $b = 0.38$ nm, and $l_p = 0.2$ nm (see also Hofmann et al. (35)) as parameters for the chain and $h = 4$ nm and $r = 2.25$ nm, as given by Horwich et al. (39), as the dimensions of the cylinder. Since the sums in Eq. 6 are dominated by small values of k (40), we included only the first five terms of the two sums in Eq. 7. The calculation results in $F_{Chain} = 8\ k_BT$.

To compute the entropy of a hard sphere inside a cylinder we used an expression for the volume fraction, f, of the confining cylinder with the volume, V_C, that is accessible to a sphere with radius a. The volume fraction is given by

$$f = \frac{\pi(r - a)^2(h - a)}{\pi r^2 h}. \quad (8)$$

The radius of the compact denatured rhodanese (a) was obtained from the Stokes radius of denatured CAM-Rho (see Results). Finally, the free energy

of confinement (in k_BT) is given by $F_{Sphere} = -\ln(f)$. For rhodanese, we obtain $F_{Sphere} = 5\ k_BT$.

RESULTS

The conformation of denatured CypA and Rho free in solution

To probe the conformational ensembles of denatured CypA and Rho, five variants of each protein with different interdye separation were investigated. Alexa Fluor 488 and Alexa Fluor 594 were attached to each variant as donor and acceptor, respectively, to obtain information on the distance between amino acid residues i and j of fluorophore attachment. The distance-related change of the mean transfer efficiency, $\langle E \rangle$, as a function of the number of peptide bonds between the fluorophores, $|i - j|$, can be used to characterize the conformational distribution of the denatured proteins (41,42). At high concentrations of GdmCl, which effectively suppresses interactions within denatured proteins (35,43), $\langle E \rangle$ decreases with increasing sequence separation of the dyes for both proteins (Fig. 2 *b*), as expected for fully unfolded proteins based on the length scaling of polymer models for expanded and unstructured chains (41,44).

However, to understand the effect of GroEL on the conformation of proteins, it is crucial to compare denatured CypA and Rho under near-physiological conditions in the absence of GroEL. To this end, we transiently populate the denatured proteins at low denaturant concentrations (0.4 M GdmCl) in a microfluidic mixing device designed specifically for kinetic single-molecule experiments (17,33). The proteins in 4 M GdmCl were mixed with physiological buffer within a dead time of 4 ms (33), and both proteins were still fully denatured 125 ms after transfer to 0.4 M GdmCl (Fig. 2 *a* and Fig. S1 in the Supporting Material) (19,44). Correspondingly, only two peaks are observed in the transfer efficiency histograms for each variant: the peak at high E results from double-labeled denatured protein, and the peak near $E = 0$ results from molecules lacking an active acceptor dye, a peak that can be eliminated by alternating excitation of donor and acceptor (45) (Fig. 2 *a*).

For denatured CypA at 0.4 M GdmCl, $\langle E \rangle$ of all variants is substantially higher than at 7.3 M GdmCl owing to the formation of interactions within the polypeptide that result in a compaction of the denatured protein (44,46,47). However, the transfer efficiencies of the different CypA variants still decrease with increasing sequence separation of the fluorophores, indicating that no or little specific tertiary structure is formed in denatured CypA (Fig. 2 *b*). In contrast to CypA, the denatured Rho variants at 0.4 M GdmCl show unusually high transfer efficiencies of $\langle E \rangle > 0.8$, independent of sequence separation from 39 to 159 peptide bonds (Fig. 2 *b*). The same result was found for CAM-Rho, a chemically modified version of rhodanese that resembles the denatured state of rhodanese but is unable to fold (Fig. S2). These high

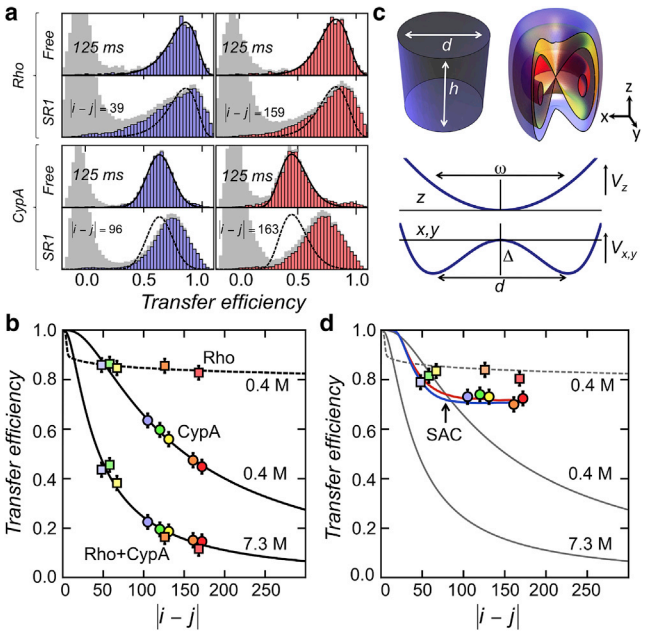

FIGURE 2 Transfer efficiency histograms and mean transfer efficiencies for denatured CypA and Rho free in solution and bound to GroEL-SR1. (*a*) Histograms for the shortest (*blue*) and longest (*red*) interdye variants of denatured Rho and CypA free in solution at 125 ms after mixing with native buffer in the microfluidic device (final GdmCl concentration, 0.4 M) and bound to GroEL-SR1. Solid lines are fits with a log-normal distribution, which are also shown as dashed lines in the histograms of CypA and Rho bound to GroEL-SR1. (*b*) Mean transfer efficiency of denatured Rho (*squares*) and CypA (*circles*) variants as a function of the sequence separation between the fluorophores at two different GdmCl concentrations. The length of the fluorophore linker was estimated to be equivalent to nine additional peptide bonds (35). Solid lines are fits with the ideal chain model with persistence length l_p as the only free parameter. The dashed line is a fit with the ideal chain model with the persistence length and the length-scaling exponent (ν) as free parameters (see the Supporting Material). (*c*) Confining geometries used in SAC simulations. Shown are the repulsive cylinder (*upper left*) and the potential with attractive interactions between the chain and the confining walls (*upper right*). The potential is harmonic in the z-direction (V_z) with spring constant ω^{-2}, and the potential in the xy-axis ($V_{x,y}$) is a double-well potential with barrier height Δ and distance d between the two wells. (*d*) Mean transfer efficiencies of denatured Rho (*squares*) and CypA (*circles*) variants bound to SR1 are shown as a function of the sequence separation between the fluorophores. Red and blue lines are the result of SAC simulations of a chain with 167 amino acids inside a cylinder (*red*) ($d = 7$ nm and $h = 8$ nm) and inside a potential (*blue*) ($\Delta = 1\ k_BT$, $d = 4$ nm, and $\omega = 2$ nm) that best describe the measured transfer efficiencies (see Supporting Material). The gray lines are identical to the fits in *b* and are shown here for comparison. Error bars (± 0.03) in *b* and *d* represent our estimate of the uncertainty in the determination of transfer efficiencies (see Materials and Methods). To see this figure in color, go online.

transfer efficiencies and their independence of sequence separation cannot be reconciled with the properties of an expanded unstructured chain but rather suggest a very compact conformation (42) of denatured Rho under near-physiological conditions. Indeed, previous experiments have even suggested the formation of rather specific structure in denatured Rho at 0.4 M GdmCl (27). CypA and Rho can therefore be considered representatives of two

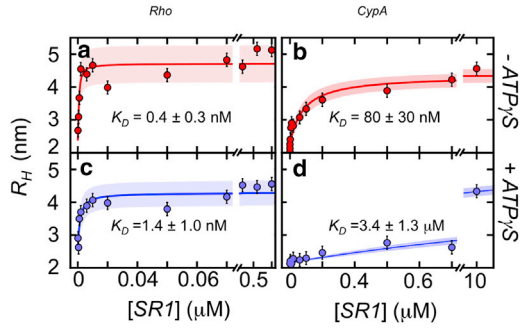

FIGURE 3 Binding of CypA and Rho by GroEL-SR1. Average Stokes radii (R_H) of CAM-Rho (E77C/K135C-A488/A594) (*a*) and CypA (V2C-A488) (*b*) as a function of the concentration of GroEL-SR1, determined using 2f-FCS at 22°C. (*c* and *d*) Same as in *a* and *b*, but in the presence of 1 mM ATPγS. The shaded regions indicate the error band resulting from the propagation of the errors in the fit parameters (Eq. 2 in Materials and Methods). To see this figure in color, go online.

extremes in the substrate spectrum of GroEL: random-coil-like, with large conformational entropy on the one hand (CypA), and compact, partially structured, with low conformational entropy on the other (Rho). This characteristic difference between CypA and Rho is our starting point for investigating the role of denatured state properties on binding and encapsulation in the chaperonin GroEL.

The conformational distribution of CypA and Rho in complex with single-ring GroEL

In the absence of ATP and under physiological conditions, both CypA and Rho bind strongly to GroEL with dissociation constants of $K_D = 0.4 \pm 0.3$ nM for CAM-Rho and $K_D = 80 \pm 30$ nM for CypA, as determined by 2f-FCS (34) on the single-ring variant of GroEL (SR1) (Fig. 3, *a* and *b*). Comparable binding affinities have been found for DM-MBP ($K_D = 60$ nM) (48), a variant of maltose binding protein, and α-lactalbumin ($K_D = 27$ nM) (49). In complex with SR1, the transfer efficiency histograms of all variants of CypA and Rho are broader than those of the free denatured proteins under physiological conditions (Fig. 2 *a*), predominantly as a result of the increased fluorescence anisotropy of the donor and acceptor fluorophores (17,27) (Fig. S3).

A comparison of the mean transfer efficiency before (Fig. 2 *b*) and after binding to SR1 (Fig. 2 *d*) reveals a striking difference between CypA and Rho. The values of $\langle E \rangle$ for Rho are virtually unaltered on binding to SR1 (Fig. 2, *b* and *d*), implying that Rho remains compact in complex with the chaperone. The values of $\langle E \rangle$ for the CypA variants bound to SR1, however, are strongly increased compared to those of free denatured CypA (Fig. 2, *b* and *d*) and become virtually independent of $|i-j|$ (Fig. 2 *d*), reminiscent of the behavior of compact denatured Rho. This change in the length scaling of $\langle E \rangle$ on binding to GroEL indicates a substantial effect of confinement on denatured CypA. Both the higher value of the transfer efficiencies and their independence of sequence separation indicate that the CypA chain is more compact in complex with GroEL than free in solution. However, the transfer efficiencies are still lower than those of Rho in complex with SR1, indicating a looser conformation of CypA compared to Rho (Fig. 2 *d*).

To elucidate whether the observed transfer efficiencies of CypA bound to GroEL are still in accord with a largely unstructured polypeptide, we used simulations of self-avoiding random chains (SACs) inside confining geometries with the dimensions of the cavity of GroEL with and without including attractive interactions with the cavity walls (Fig. 2 *c* and Fig. S5). Indeed, confining a SAC with the length of CypA (167 aa) to a small volume qualitatively reproduces the effect of $|i-j|$ -independent transfer efficiencies (Fig. 2 *d*), suggesting that confinement inside the central hole of GroEL, the location of the substrate binding sites, sufficiently explains the altered chain statistics of CypA in complex with SR1.

Even though both CypA and Rho bind to SR1 with nanomolar affinity (Fig. 3, *a* and *b*), the difference between their free energies of binding is significant ($\Delta\Delta G_{\text{Rho-CypA}} = 5 \pm 1\ k_BT$). Considering the difference in the conformations of both substrates free and bound to SR1 (Fig. 2, *b* and *d*), we estimated the impact of the different denatured-state properties on the free energies of SR1 binding by computing the entropy cost of confining Rho and CypA in the interior of GroEL. Since denatured Rho is very compact, both in solution and also in complex with SR1 (Fig. 2, *b* and *d*), a lower limit for the entropy cost of GroEL binding is estimated from the process of trapping a sphere in the interior of GroEL. We modeled GroEL as a cylindrical cavity with a radius of 2.25 nm and a height of 4 nm (39) (see Materials and Methods) and estimated the radius of gyration of denatured Rho based on the Stokes radius of denatured CAM-Rho ($R_H = 2.7$ nm). Assuming that compact denatured Rho has a spherical shape, we obtain $R_G \approx 2$ nm using $R_G/R_H = (3/5)^{1/2}$ (50). In contrast, CypA is approximated as an ideal chain, which allows a straightforward calculation of the entropy cost on confinement in the same cylinder (see Materials and Methods). This approximation is supported by the length-scaling exponent (ν) of CypA, which has recently been found to be close to the value expected for an ideal chain ($\nu = 0.5$) (35). We note that neither estimate includes effects arising from solvent entropy, such as the displacement of water molecules during binding to GroEL. With these approximations, the difference in conformational entropy ($-T\Delta\Delta S_{\text{conf}}$) between the confinement of CypA and Rho inside the central hole of SR1 is estimated to be ~3 k_BT and varies between 2.1 k_BT and 4.5 k_BT with a change in the cylinder volume of ±25%. The comparison of the experimentally observed free-energy difference for SR1 binding ($\Delta\Delta G_{\text{Rho-CypA}} = 6 \pm 1\ k_BT$) with our estimate of ~3 k_BT obtained from polymer theory indicates that about half of the destabilization of the CypA-SR1 complex relative to

the Rho-SR1 can already be explained by the loss in conformational entropy upon confinement, which suggests that the polymeric properties of denatured substrates can significantly affect the binding of denatured substrates to GroEL. The remaining free-energy difference of 2 k_BT is likely to result from a greater interaction enthalpy of Rho with GroEL owing to its longer sequence, which allows more contacts with GroEL to be made.

Dynamics and thermodynamics of CypA and Rho interactions with GroEL

The different effects of GroEL on the conformation of CypA and Rho (Fig. 2, *b* and *d*) suggest that the kinetics of binding may also be different for the two denatured proteins. We used ensemble stopped-flow fluorescence of donor-labeled CypA and Rho to monitor the binding kinetics in the time regime of milliseconds to seconds. The binding to SR1 changes the fluorescence intensity of AlexaFluor 488 due to PET (51) to aromatic amino acids such as tryptophan and tyrosine in Rho and CypA, respectively. Compared to single-molecule FRET, PET is sensitive for local distance changes, which is especially advantageous for the study of protein dynamics in confined spaces where large distance changes cannot occur.

Mixing of rhodanese and cyclophilin with SR1 under pseudo-first-order conditions results in single-exponential binding kinetics with increasing fluorescence intensity for Rho and rising fluorescence intensity for Cyp (Fig. 4, *b* and *c*). However, the observed rate constant for binding, k, increases nonlinearly with increasing concentration of SR1 and saturates at high SR1 concentrations (Fig. 4, *d* and *e*), which indicates the presence of a second kinetic step that is rate-limiting under these conditions. A generalized binding model (52) that includes two steps, the diffusion-controlled formation of a transient-encounter complex between GroEL and the denatured substrate (S), [GroEL•S]*, followed by a conformational adaptation of the denatured proteins to the GroEL surface, describes this behavior quantitatively (Fig. 4 *a*). The rate constant for the adaptation process, k_{max}, can then be obtained as the asymptotic limit of the binding constant, k, approached at high SR1 concentrations (see Materials and Methods). Whereas $k_{max} = 105 \pm 8\ s^{-1}$ at 25°C for CypA, the adaptation process is slower for Rho, with $k_{max} = 27 \pm 3\ s^{-1}$ at 25°C. The diffusive chain reconfiguration time of denatured CypA free in solution was found to be 150 ns ns-FCS (Fig. S4). Since the conformational adaptation of both denatured proteins to SR1 is several orders of magnitude slower than the diffusive chain dynamics, we conclude that a large activation barrier must be involved in the adaptation to the SR1 surface. To obtain structural information from the activation parameters of this process, we express the adaptation rate constant in terms of a generalized reaction rate equation $k_{max} = k_0 \exp(-\Delta G^{\ddagger}/RT)$, and estimate the attempt frequency (k_0) for crossing the barrier ($\Delta G^{\ddagger}$) based on the chain reconfiguration times of denatured Cyp and Rho determined in free solution to be $k_0 \approx 1\ \mu s^{-1}$ (Supporting Material) (53,54). By combining this estimate for the preexponential factor with the binding kinetics as a function of temperature (Fig. 4, *d* and *e*), we obtain the change in activation enthalpy ($\Delta H^{\ddagger}$), activation entropy ($\Delta S^{\ddagger}$), and heat capacity ($\Delta C_p^{\ddagger}$) during adaptation (Fig. 4, *f* and *g*) (see Materials and Methods).

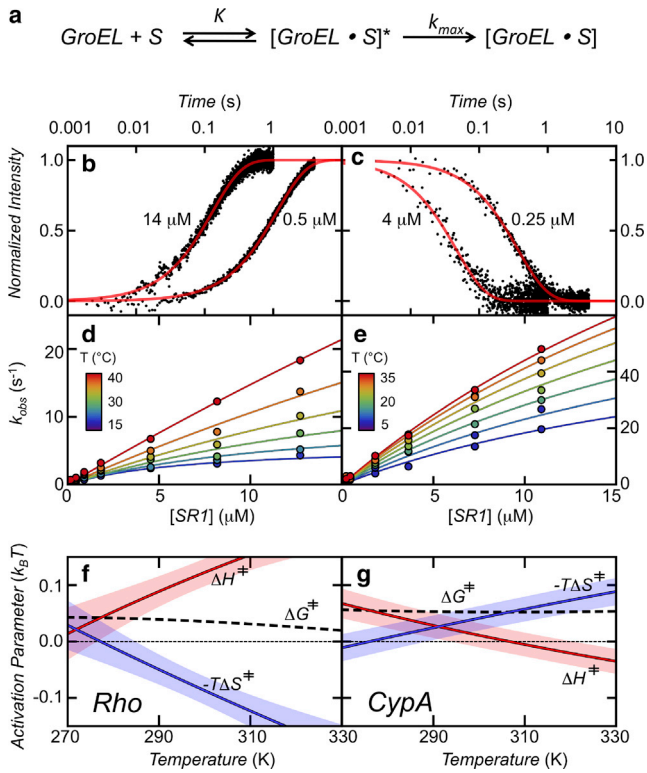

FIGURE 4 Binding and adaptation kinetics measured with stopped-flow fluorescence at 0.4 M GdmCl. (*a*) Generalized mechanism for the bimolecular reaction of substrate binding to GroEL-SR1. (*b* and *c*) Examples of progress curves for Alexa 488-labeled Rho (E285C) (*b*) and CypA (D13C/G124C) (*c*) at two concentrations of GroEL-SR1 indicated. (*d* and *e*) Change of the apparent pseudo-first-order rate constants for binding of Rho (*d*) and CypA (*e*) at different temperatures and SR1 concentrations and fits according to the model in Scheme 1 (see Materials and Methods) with the parameters $\Delta H_{eq} = -90 \pm 25$ kJ mol^{-1}, $\Delta S_{eq} = -0.44 \pm 0.08$ kJ mol^{-1} K^{-1}, $\Delta H^{\ddagger} = 85 \pm 18$ kJ mol^{-1}, $\Delta S^{\ddagger} = 0.2 \pm 0.1$ kJ mol^{-1} K^{-1}, and $\Delta C^{\ddagger} = 2.7 \pm 0.9$ kJ mol^{-1} K^{-1} for Rho, and with the parameters $\Delta H_{eq} = -8 \pm 11$ kJ mol^{-1}, $\Delta S_{eq} = -0.17 \pm 0.04$ kJ mol^{-1} K^{-1}, $\Delta H^{\ddagger} = 6 \pm 9$ kJ mol^{-1}, $\Delta S^{\ddagger} = -0.05 \pm 0.03$ kJ mol^{-1} K^{-1}, and $\Delta C^{\ddagger} = -0.7 \pm 0.2$ kJ mol^{-1} K^{-1} for CypA. The values for the activation parameters are given at $T_0 = 298$ K (see Eq. 4 in Materials and Methods). (*f* and *g*) Temperature dependence of the activation parameters for the adaptation processes for Rho (*f*) and CypA (*g*). All activation parameters are given in units of k_BT per amino acid residue. Shaded regions indicate the error of the fits in *c* and *d*, which result from the fitting-parameter error propagation. The change in the viscosity of water with increasing temperature is taken into account (see Materials and Methods). To see this figure in color, go online.

The changes in $\Delta H^{\ddagger}$ and $\Delta S^{\ddagger}$ are diametrically opposed for Rho and CypA. With increasing temperature, the

adaptation barrier for Rho is increasingly determined by enthalpy rather than entropy because of a positive heat capacity change (Fig. 4 *f*). This behavior is typical of the interaction of nonpolar solutes with water (55,56). With increasing temperature, the disorder of water clusters around hydrophobic residues increases, leading to a decrease in the entropy change upon mixing. At high temperatures, the aversion of nonpolar solutes to water is therefore mainly enthalpy-driven (55,56). For Rho, the temperature dependence of $\Delta H^{\ddagger}$ and $\Delta S^{\ddagger}$ therefore points to an exposure of hydrophobic residues in the adaptation process, indicating that changes in the hydration of these residues dominate the observed entropy change upon binding to GroEL. Although the change in quantum yield of Alexa-Fluor 488 upon binding of Rho to SR1 clearly demonstrates the presence of local conformational rearrangements in denatured Rho, the absence of an increase in activation entropy with increasing temperature, which could indicate an increasing loss in conformational entropy, suggests that confinement does not contribute much to the reaction, which is in line with the small change in the transfer efficiencies of all Rho variants on binding to GroEL. For CypA, on the other hand, the heat capacity change is negative and $\Delta S^{\ddagger}$ more and more dominates the adaptation barrier with increasing temperature (Fig. 4 *g*). Both the increasing cost of restricting the conformational distribution by GroEL-induced confinement and the net burial of hydrophobic side chains of CypA can explain this decrease in $\Delta S^{\ddagger}$. Both interpretations are in accord with the compaction of the initially well-solvated and expanded CypA chain upon binding to GroEL-SR1, as revealed by the single-molecule FRET experiments (Fig. 2, *b* and *d*).

In summary, the differences in the kinetics, thermodynamics, and transfer efficiency of GroEL binding reflect differences in the degree of compaction of denatured Rho and CypA free in solution. How do these differences affect the key step in chaperonin action, the encapsulation of both proteins upon addition of ATP and GroES?

Encapsulation of Rho versus expulsion of CypA by GroEL-GroES

We monitored the encapsulation of CypA and Rho by 2f-FCS (34) and size-exclusion chromatography (Fig. S7). The average Stokes radii of complexes of donor-labeled CypA or Rho with SR1 are dominated by the size of SR1, resulting in values of 4.5–5.3 nm (Fig. 5 *a*). Binding of ATP to GroEL is known to trigger a rotation of the apical domains, followed by an upward movement on binding of GroES (57), which concludes the encapsulation reaction. The entire process takes place within seconds (58). Upon addition of 2 mM ATP and 1 μM GroES (reflecting physiological concentrations) to the preformed Rho-SR1 complex, R_H of the fluorescent species increases from 5.3 nm to 5.9 nm, indicating that Rho is encapsulated in the central

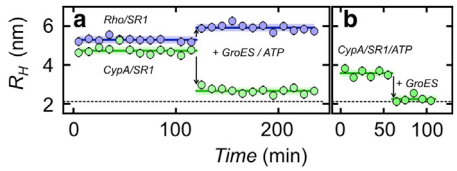

FIGURE 5 Encapsulation of Rho and release of CypA by GroEL-SR1. (*a*) Effect of the addition of 1 μM GroES and 2 mM ATP on R_H of preformed complexes of GroEL-SR1 with CypA (*green*) and Rho (*blue*) at a final concentration of 25 nM GroEL-SR1. Arrows indicate the time of addition of ATP and GroES. (*b*) R_H of CypA in the presence of 275 nM GroEL-SR1 and 2 mM ATP before and after the addition of 1 μM GroES (*arrow*). Solid lines indicate the mean of R_H. Dashed line indicates the R_H of free CypA. To see this figure in color, go online.

cavity formed by SR1 and GroES (Fig. 5 *a*). Surprisingly, however, the addition of ATP and GroES to CypA-SR1 complexes leads to a decrease of the Stokes radius to 2.6 nm, close to the Stokes radius of free CypA (2 nm) (Fig. 5 *a*). Evidently, the majority of CypA is not stably encapsulated in the cavity formed by SR1 and GroES, as also confirmed by size-exclusion chromatography (Fig. S7).

Why is CypA not encapsulated even though it binds to SR1 with nanomolar affinity? In contrast to Rho-SR1, we found that the stability of the CypA-SR1 complex is strongly diminished, by ~4 k_BT, in the presence of 1 mM ATPγS, a nonhydrolyzable ATP analog (Fig. 3, *c* and *d*). This effect has been observed for other substrate proteins (59–61), such as DM-MBP, a variant of maltose-binding protein (48). Taking this decrease in affinity into account, a simple explanation for the failure of GroEL-GroES to encapsulate CypA would be a kinetic competition of GroES binding with the ATP-induced dissociation of CypA from GroEL. Encapsulation will only be successful for those GroEL-substrate complexes where GroES happens to bind before the substrate dissociates after ATP binding. In this case, preforming the CypA-SR1-ATP complex should lead to more efficient encapsulation of CypA. At a concentration of 275 nM SR1, the ternary CypA-SR1-ATP complex is populated significantly, as revealed by the Stokes radius of 3.8 nm compared to the value of free CypA (2 nm) (Fig. 5 *b*). However, the addition of GroES does not lead to an increased encapsulation yield of CypA. Instead, the Stokes radius again decreases to 2 nm, the value obtained for free CypA (Fig. 5 *b*). These results suggest that it is not the binding of ATP that is responsible for the release of CypA but the binding of GroES.

Assuming that the binding of ATP is faster than the binding and dissociation of substrate (62), three different models can potentially explain the results. In the first model (Fig. 6 *a*, *Model 1*), binding of GroES is sterically hindered by the presence of CypA. Consequently, CypA has to leave SR1-ATP for GroES to bind. In the second model (Fig. 6 *a*, *Model 2*), GroES can associate with the CypA-SR1-ATP complex and CypA dissociates during GroES binding. This model assumes the existence of an intermediate in

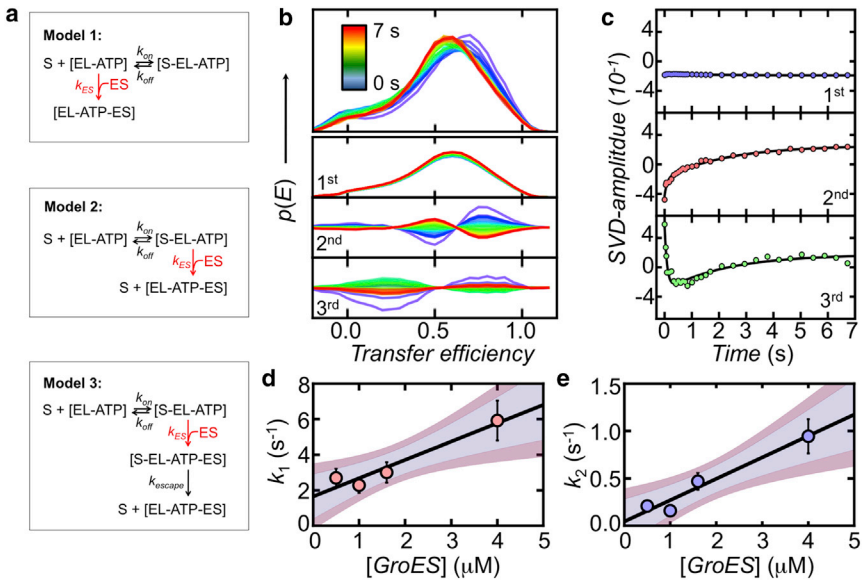

FIGURE 6 Release kinetics of CypA on addition of GroES and ATP. (*a*) Three different models for CypA release, with binding of GroES highlighted in red. (*b*) Transfer efficiency histograms (*upper*) for FRET-labeled CypA (V2C/K154C) bound to GroEL-SR1 at different times after mixing with 2 mM ATP and 1 μM GroES in the microfluidic device (see Materials and Methods) and the first three resulting singular value decomposition components (*lower*). The peak at zero transfer efficiency was removed using pulsed interleaved excitation (45). (*c*) First three amplitude vectors of the SVD shown reflect the progress of the reaction. Solid lines are global fits of the three components with double-exponential decays. (*d* and *e*) GroES dependence of the fast (*d*) and slow (*e*) phases of CypA release, obtained for CypA variant D13C/G124C. To see this figure in color, go online.

which GroES is in a predocking position before it finally binds tightly to the R-state of SR1. Evidence for such an intermediate comes from recent cryo-electron microscopy studies, which identified at least two different conformations of GroEL-ATP, one of which would allow an interaction with GroES (63). As an alternative (Fig. 6 *a*, *Model 3*), denatured CypA is successfully encapsulated but leaves the SR1-ATP-GroES complex at a later stage. This mechanism is supported by the observation that substrate proteins can escape the cage formed by GroEL-GroES even after the encapsulation has taken place (64). To distinguish between these mechanisms, we investigated the kinetics of CypA dissociation from the GroEL-GroES complex using smFRET in combination with microfluidic mixing. Whereas a GroES-driven expulsion of CypA (Models 1 and 2) would occur within 10 s after the addition of GroES and ATP, an escape from the SR1-ATP-GroES cavity (Model 3) is expected to occur in the time regime of several minutes (64).

Kinetics of CypA expulsion from the SR1-ATP-GroES complex

In a time-resolved experiment using microfluidic mixing, we can monitor the kinetics of CypA dissociation during binding of ATP and GroES using smFRET (Fig. 6, *b* and *c*). A sample solution containing CypA-SR1 complexes was rapidly mixed with buffer containing ATP and GroES, and transfer efficiency histograms were obtained at different times after initiating the reaction (Fig. 6 *b*). For all CypA variants, a model-free analysis of the data using multidimensional singular value decomposition (17) (Fig. 6, *b* and *c*) resulted in three significant components (Fig. S6) with clearly double-exponential kinetics and two apparent rate constants ($k_1 = 10.5\ s^{-1}$, $k_2 = 0.44\ s^{-1}$) (Fig. 6 *c*), implying at least a three-state mechanism for the dissociation of CypA. Most important, the rate constant (k_2) for the slow process suggests that ~90% of the SR1-bound CypA is already dissociated 5 s after mixing with GroES and ATP. The formation of the ternary SR1-ATP-GroES complex in the presence of substrate has previously been shown to occur on the same timescale (58), suggesting that CypA leaves GroEL during GroES binding. A slow escape after encapsulation (Fig. 6 *a*, *Model 3*) can therefore be excluded.

A distinction between Models 1 and 2 is possible from the GroES-concentration dependence of the CypA release kinetics. In Model 1, GroES only binds to SR1 without CypA bound. Correspondingly, the kinetics of CypA release are determined by the spontaneous dissociation of CypA and the rate constants for the two observed kinetic phases (k_1, k_2) should not depend on the GroES concentration. In contrast, if CypA is released during binding of GroES (Fig. 6 *a*, *Model 2*), CypA dissociation will accelerate with increasing GroES concentrations. Experimentally, we find an increase in the rate constants for the fast (k_1) and slow (k_2) processes with increasing concentration of GroES (Fig. 6, *d* and *e*), indicating that GroES binding and CypA release are coupled processes. Hence, only Model 2 is in accord with the experimental data, i.e., CypA is released during the process of GroES binding.

Encapsulation versus expulsion: the role of substrate properties

Since GroES binding triggers the release of CypA, the interaction free energy between CypA and SR1 is apparently insufficient to resist the forces associated with the rearrangement of the apical domains of SR1 on GroES binding (63). However, what are the relative contributions of enthalpic or hydrophobic interactions between chaperone and substrate

protein and the conformational entropy for encapsulation of a disordered chain like CypA? To test the importance of the interaction strength between CypA and SR1 for encapsulation, we increased the hydrophobicity of the CypA sequence by decorating it with the amino-reactive hydrophobic linker LC-SPDP, thus forming LC-CypA. As expected, LC-CypA binds stably to SR1, resulting in a Stokes radius of 5.3 nm for the LC-CypA-SR1 complex (Fig. 7 *e*). It is important to point out that after the addition of GroES and ATP to preformed LC-CypA-SR1 complexes, we found a significantly increased encapsulation efficiency compared to that observed for CypA (Fig. 7, *d* and *e*). The Stokes radius of the free protein measured with 2f-FCS revealed that LC-CypA is more compact by ~0.6 nm than unmodified CypA in 0.5 M GdmCl (Fig. 7, *a* and *b*). This reduction in the Stokes radius is explained by the greater hydrophobicity of the sequence, which promotes a hydrophobic collapse of the chain (44,47). These observations raise the question of whether the compaction of the LC-CypA chain, as compared to CypA, lowers the entropic cost for encapsulation and is thus responsible for the increased encapsulation yield. We therefore cross-linked CypA intramolecularly by oxidizing tris-bipyridylruthenium(II) to tris-bipyridylruthenium(III) using laser-induced photolysis (see Materials and Methods) (38). The oxidized Ru^{3+} preferentially oxidizes aromatic amino acid residues that then react nonspecifically with nucleophilic groups such as the primary ε-amino groups of lysine residues, which should only lead to a marginal change in overall hydrophobicity. 2fFCS shows that at low concentrations of GdmCl (0.5 M), cross-linked CypA (Ru-CypA) (Fig. 7 *c*) is more compact by ~0.4 nm than unmodified CypA (Fig. 7 *a*) and forms a stable complex with SR1 (Fig. 7 *f*). However, the addition of ATP and GroES leads to a rapid drop in the Stokes radius similar to that of non-cross-linked CypA (Fig. 7, *d* and *f*), indicating that the encapsulation efficiency of Ru-CypA is not markedly increased compared to CypA. The result therefore suggests that a reduction in the entropy cost of encapsulation is not the key determinant for greater encapsulation efficiency. Even though LC-CypA is more collapsed owing to its greater hydrophobicity, it is the increased hydrophobicity, and not the smaller dimensions, that facilitate its encapsulation.

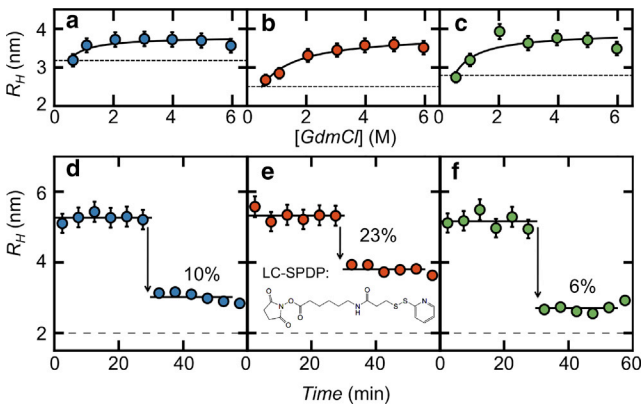

FIGURE 7 Effect of intramolecular cross linking and chemical modifications of CypA on encapsulation efficiency. (*a–c*) The Stokes radii (R_H) from 2f-FCS of Alexa 488-labeled CypA (*a*), LC-CypA (*b*), and Ru-CypA (*c*) (variant K28C) are shown as a function of the GdmCl concentration. Black solid lines are fits with a denaturant binding isotherm. Black dashed lines indicate the Stokes radius extrapolated to 0.5 M GdmCl. (*d–f*) Effect of the addition of 2 μM GroES and 1 mM ATP on the R_H of preformed SR1 in complex with CypA (*d*), LC-CypA (*e*), and Ru-CypA (*f*). Arrows indicate the time of addition of 1 mM ATP and 2 μM GroES. The chemical structure of the LC-SPDP is shown as an inset in *e*. To see this figure in color, go online.

DISCUSSION

CypA has a low conformational stability, is aggregation-prone at high protein concentrations (29), and binds to GroEL with high affinity (Fig. 3 *b*). However, it fails to become encapsulated in the chaperonin cavity (Fig. 5). This observation is very surprising, since CypA meets all sequence criteria for a GroEL substrate. With a length of 167 amino acids (18 kD), it is well within the size limits of typical substrate proteins (Fig. 1 *c*), and it has a mean hydrophobicity and net charge similar to those of Rho and other identified GroEL substrates (Fig. 1 *b*). Stan and co-workers identified hydrophobic GroEL-binding motifs based on a sequence comparison of 284 GroEL substrates (18) (Fig. 1 *d*), and recent NMR-relaxation studies have demonstrated that the amyloid peptide (Aβ-40) indeed interacts with GroEL via the predicted consensus sequence (65). Based on sequence analysis, we identified three hydrophobic GroEL-binding motifs in CypA, which corresponds to a total of 17 amino acids relevant for the CypA-GroEL interactions, which is within the range reported for typical GroEL substrates (6,7,18) (Fig. 1 *d*). The question therefore arises, which aspects determine the success of chaperonin encapsulation?

Rho and CypA differ substantially in their chain lengths and in the compactness of their denatured-state ensembles. The more expanded conformation of CypA is expected to result in an entropy cost for binding to GroEL that is higher by ~3 k_BT than that of Rho, as reflected in the entropy-dominated adaptation barrier that has to be crossed for a stable interaction of CypA with SR1 (Fig. 4 *f*). Correspondingly, rearrangements in the apical domains of GroEL upon GroES binding (57) might affect the interactions between CypA and GroEL more than those between Rho and GroEL, which would favor the release of CypA. However, the intramolecularly cross-linked and more compact Ru-CypA variant demonstrates that the encapsulation efficiency does not increase with increasing compaction of CypA (Fig. 7 *f*), making the higher entropy cost unlikely to be the dominant reason for the failing encapsulation of CypA. Only if the hydrophobicity of CypA is increased, as realized in the LC-CypA variant, can the encapsulation efficiency be improved

(Fig. 7 *e*). Thus, hydrophobicity facilitates both collapse and encapsulation, but compaction of the substrate protein alone is insufficient for increasing the encapsulation yield.

Our kinetic analysis shows that unmodified CypA leaves the GroEL-GroES complex in a transient state in which GroES is already associated but not yet tightly bound to GroEL, a type of conformation that has recently been suggested based on cryo-electron microscopy (63) and may serve as a checkpoint for substrate discrimination. For GroES to complete the binding process, its mobile loops have to interact with the apical domains of GroEL (63), and the interactions with the substrate have to be released. This leads to the dissociation of CypA; but how is premature substrate release prevented for Rho and other GroEL substrates? A recent model for the encapsulation process of denatured substrate proteins suggests that the C-terminal tails at the base of the GroEL cavity reduce premature substrate protein escape while the apical domains move to interact strongly with GroES (20). Indeed, the last 17 amino acids of the disordered C-terminal tail of GroEL (23 aa) show a high mean hydrophobicity of 0.587 (Fig. 1 *b*). Clearly, the interactions between these disordered tails and substrate proteins will depend on the total number and accessibility of nonpolar groups in the denatured protein. Given the similar mean hydrophobicities of Rho and CypA, the longer Rho chain is expected to interact more strongly with the C-terminal tails than the shorter CypA chain. Thus, our findings are in accord with the model of Chen et al. (20) and suggest that in addition to the presence of an upper limit for the interaction strength between a substrate protein and GroEL, as suggested by the iterative annealing model (66,67), there also exists a lower limit.

In summary, our results demonstrate that high affinity of a substrate protein for GroEL does not necessarily lead to its encapsulation and folding inside the chaperonin cage. Rather, the strength of the hydrophobic interactions of substrate proteins with a transient GroEL-GroES complex is decisive for avoiding premature release of the denatured protein.

SUPPORTING MATERIAL

Supporting Materials and Methods, seven figures, and one table are available at http://www.biophysj.org/biophysj/supplemental/S0006-3495(14)01153-9.

We thank G. Lorimer for the gift of the SR1 plasmid. We also thank E. Shakhnovich and A. Horwich for helpful comments and Stephan Benke for help with cross-linking experiments.

This work was supported by a Starting Independent Researcher grant from the European Research Council (to B.S.) the Swiss National Center for Competence in Research for Structural Biology (to B.S.), the Swiss National Science Foundation (to B.S.), the Human Frontier Science Program (to E.A.L. and B.S.), and the National Science Foundation (to E.A.L.).

SUPPORTING CITATIONS

References (68–73) appear in the Supporting Material.

REFERENCES

1. Thirumalai, D., and G. H. Lorimer. 2001. Chaperonin-mediated protein folding. *Annu. Rev. Biophys. Biomol. Struct.* 30:245–269.
2. Fenton, W. A., and A. L. Horwich. 2003. Chaperonin-mediated protein folding: fate of substrate polypeptide. *Q. Rev. Biophys.* 36:229–256.
3. Bukau, B., J. Weissman, and A. Horwich. 2006. Molecular chaperones and protein quality control. *Cell.* 125:443–451.
4. Hartl, F. U., A. Bracher, and M. Hayer-Hartl. 2011. Molecular chaperones in protein folding and proteostasis. *Nature.* 475:324–332.
5. Coyle, J. E., F. L. Texter, …, S. E. Radford. 1999. GroEL accelerates the refolding of hen lysozyme without changing its folding mechanism. *Nat. Struct. Biol.* 6:683–690.
6. Houry, W. A., D. Frishman, …, F. U. Hartl. 1999. Identification of in vivo substrates of the chaperonin GroEL. *Nature.* 402:147–154.
7. Kerner, M. J., D. J. Naylor, …, F. U. Hartl. 2005. Proteome-wide analysis of chaperonin-dependent protein folding in *Escherichia coli*. *Cell.* 122:209–220.
8. Shimamura, T., A. Koike-Takeshita, …, S. Iwata. 2004. Crystal structure of the native chaperonin complex from *Thermus thermophilus* revealed unexpected asymmetry at the *cis*-cavity. *Structure.* 12:1471–1480.
9. Hartl, F. U., and M. Hayer-Hartl. 2002. Molecular chaperones in the cytosol: from nascent chain to folded protein. *Science.* 295:1852–1858.
10. Zhou, H. X., and K. A. Dill. 2001. Stabilization of proteins in confined spaces. *Biochemistry.* 40:11289–11293.
11. Takagi, F., N. Koga, and S. Takada. 2003. How protein thermodynamics and folding mechanisms are altered by the chaperonin cage: molecular simulations. *Proc. Natl. Acad. Sci. USA.* 100:11367–11372.
12. Betancourt, M. R., and D. Thirumalai. 1999. Exploring the kinetic requirements for enhancement of protein folding rates in the GroEL cavity. *J. Mol. Biol.* 287:627–644.
13. Klimov, D. K., D. Newfield, and D. Thirumalai. 2002. Simulations of β-hairpin folding confined to spherical pores using distributed computing. *Proc. Natl. Acad. Sci. USA.* 99:8019–8024.
14. Mittal, J., and R. B. Best. 2008. Thermodynamics and kinetics of protein folding under confinement. *Proc. Natl. Acad. Sci. USA.* 105:20233–20238.
15. Hayer-Hartl, M., and A. P. Minton. 2006. A simple semiempirical model for the effect of molecular confinement upon the rate of protein folding. *Biochemistry.* 45:13356–13360.
16. Tang, Y.-C., H.-C. Chang, …, M. Hayer-Hartl. 2006. Structural features of the GroEL-GroES nano-cage required for rapid folding of encapsulated protein. *Cell.* 125:903–914.
17. Hofmann, H., F. Hillger, …, B. Schuler. 2010. Single-molecule spectroscopy of protein folding in a chaperonin cage. *Proc. Natl. Acad. Sci. USA.* 107:11793–11798.
18. Jewett, A. I., A. Baumketner, and J. E. Shea. 2004. Accelerated folding in the weak hydrophobic environment of a chaperonin cavity: creation of an alternate fast folding pathway. *Proc. Natl. Acad. Sci. USA.* 101:13192–13197.
19. Sirur, A., and R. B. Best. 2013. Effects of interactions with the GroEL cavity on protein folding rates. *Biophys. J.* 104:1098–1106.
20. Chen, D.-H., D. Madan, …, H. S. Rye. 2013. Visualizing GroEL/ES in the act of encapsulating a folding protein. *Cell.* 153:1354–1365.
21. Fischer, G., B. Wittmann-Liebold, …, F. X. Schmid. 1989. Cyclophilin and peptidyl-prolyl *cis-trans* isomerase are probably identical proteins. *Nature.* 337:476–478.
22. Kallen, J., C. Spitzfaden, …, M. D. Walkinshaw. 1991. Structure of human cyclophilin and its binding site for cyclosporin A determined by X-ray crystallography and NMR spectroscopy. *Nature.* 353:276–279.
23. Nieba-Axmann, S. E., M. Ottiger, …, A. Plückthun. 1997. Multiple cycles of global unfolding of GroEL-bound cyclophilin A evidenced by NMR. *J. Mol. Biol.* 271:803–818.

24. Mendoza, J. A., E. Rogers, …, P. M. Horowitz. 1991. Chaperonins facilitate the in vitro folding of monomeric mitochondrial rhodanese. *J. Biol. Chem.* 266:13044–13049.

25. Jordan, I. K., F. A. Kondrashov, …, S. Sunyaev. 2005. A universal trend of amino acid gain and loss in protein evolution. *Nature.* 433:633–638.

26. Stan, G., B. R. Brooks, …, D. Thirumalai. 2006. Residues in substrate proteins that interact with GroEL in the capture process are buried in the native state. *Proc. Natl. Acad. Sci. USA.* 103:4433–4438.

27. Hillger, F., D. Hänni, …, B. Schuler. 2008. Probing protein-chaperone interactions with single-molecule fluorescence spectroscopy. *Angew. Chem. Int. Ed. Engl.* 47:6184–6188.

28. Langer, T., G. Pfeifer, …, F. U. Hartl. 1992. Chaperonin-mediated protein folding: GroES binds to one end of the GroEL cylinder, which accommodates the protein substrate within its central cavity. *EMBO J.* 11:4757–4765.

29. Zahn, R., C. Spitzfaden, …, A. Plückthun. 1994. Destabilization of the complete protein secondary structure on binding to the chaperone GroEL. *Nature.* 368:261–265.

30. Koculi, E., R. Horst, …, K. Wüthrich. 2011. Nuclear magnetic resonance spectroscopy with the stringent substrate rhodanese bound to the single-ring variant SR1 of the E. coli chaperonin GroEL. *Protein Sci.* 20:1380–1386.

31. Schuler, B. 2007. Application of single molecule Förster resonance energy transfer to protein folding. *Methods Mol. Biol.* 350:115–138.

32. Chen, H., S. S. Ahsan, …, W. W. Webb. 2010. Mechanisms of quenching of Alexa fluorophores by natural amino acids. *J. Am. Chem. Soc.* 132:7244–7245.

33. Pfeil, S. H., C. E. Wickersham, …, E. A. Lipman. 2009. A microfluidic mixing system for single-molecule measurements. *Rev. Sci. Instrum.* 80:055105.

34. Dertinger, T., V. Pacheco, …, J. Enderlein. 2007. Two-focus fluorescence correlation spectroscopy: a new tool for accurate and absolute diffusion measurements. *ChemPhysChem.* 8:433–443.

35. Hofmann, H., A. Soranno, …, B. Schuler. 2012. Polymer scaling laws of unfolded and intrinsically disordered proteins quantified with single-molecule spectroscopy. *Proc. Natl. Acad. Sci. USA.* 109: 16155–16160.

36. Soranno, A., B. Buchli, …, B. Schuler. 2012. Quantifying internal friction in unfolded and intrinsically disordered proteins with single-molecule spectroscopy. *Proc. Natl. Acad. Sci. USA.* 109:17800–17806.

37. Likhachev, E. R. 2003. Dependence of water viscosity on temperature and pressure. *Tech. Phys.* 48:514–515.

38. Fancy, D. A., and T. Kodadek. 1999. Chemistry for the analysis of protein-protein interactions: rapid and efficient cross-linking triggered by long wavelength light. *Proc. Natl. Acad. Sci. USA.* 96:6020–6024.

39. Horwich, A. L., G. W. Farr, and W. A. Fenton. 2006. GroEL-GroES-mediated protein folding. *Chem. Rev.* 106:1917–1930.

40. Zhou, H. X. 2008. Protein folding in confined and crowded environments. *Arch. Biochem. Biophys.* 469:76–82.

41. Hoffmann, A., A. Kane, …, B. Schuler. 2007. Mapping protein collapse with single-molecule fluorescence and kinetic synchrotron radiation circular dichroism spectroscopy. *Proc. Natl. Acad. Sci. USA.* 104:105–110.

42. Tran, H. T., A. Mao, and R. V. Pappu. 2008. Role of backbone-solvent interactions in determining conformational equilibria of intrinsically disordered proteins. *J. Am. Chem. Soc.* 130:7380–7392.

43. Sherman, E., and G. Haran. 2006. Coil-globule transition in the denatured state of a small protein. *Proc. Natl. Acad. Sci. USA.* 103:11539–11543.

44. Reference deleted in proof.

45. Müller, B. K., E. Zaychikov, …, D. C. Lamb. 2005. Pulsed interleaved excitation. *Biophys. J.* 89:3508–3522.

46. O'Brien, E. P., G. Ziv, …, D. Thirumalai. 2008. Effects of denaturants and osmolytes on proteins are accurately predicted by the molecular transfer model. *Proc. Natl. Acad. Sci. USA.* 105:13403–13408.

47. Haran, G. 2012. How, when and why proteins collapse: the relation to folding. *Curr. Opin. Struct. Biol.* 22:14–20.

48. Sharma, S., K. Chakraborty, …, F. U. Hartl. 2008. Monitoring protein conformation along the pathway of chaperonin-assisted folding. *Cell.* 133:142–153.

49. Li, Y., Z. Zheng, …, L. Chen. 2010. Analysis of peptides and proteins in their binding to GroEL. *J. Pept. Sci.* 16:693–700.

50. Grosberg, A., and D. Kuznetsov. 1992. Quantitative theory of the globule-to-coil transition. 4. Comparison of theoretical results with experimental data. *Macromolecules.* 25:1996–2003.

51. Doose, S., H. Neuweiler, and M. Sauer. 2009. Fluorescence quenching by photoinduced electron transfer: a reporter for conformational dynamics of macromolecules. *ChemPhysChem.* 10:1389–1398.

52. Schreiber, G. 2002. Kinetic studies of protein-protein interactions. *Curr. Opin. Struct. Biol.* 12:41–47.

53. Kubelka, J., J. Hofrichter, and W. A. Eaton. 2004. The protein folding "speed limit". *Curr. Opin. Struct. Biol.* 14:76–88.

54. Nettels, D., I. V. Gopich, …, B. Schuler. 2007. Ultrafast dynamics of protein collapse from single-molecule photon statistics. *Proc. Natl. Acad. Sci. USA.* 104:2655–2660.

55. Dill, K. A. 1990. Dominant forces in protein folding. *Biochemistry.* 29:7133–7155.

56. Privalov, P. L., and S. J. Gill. 1988. Stability of protein structure and hydrophobic interaction. *Adv. Protein Chem.* 39:191–234.

57. Clare, D. K., D. Vasishtan, …, H. R. Saibil. 2012. ATP-triggered conformational changes delineate substrate-binding and -folding mechanics of the GroEL chaperonin. *Cell.* 149:113–123.

58. Motojima, F., C. Chaudhry, …, A. L. Horwich. 2004. Substrate polypeptide presents a load on the apical domains of the chaperonin GroEL. *Proc. Natl. Acad. Sci. USA.* 101:15005–15012.

59. Viitanen, P. V., G. K. Donaldson, …, A. A. Gatenby. 1991. Complex interactions between the chaperonin 60 molecular chaperone and dihydrofolate reductase. *Biochemistry.* 30:9716–9723.

60. Martin, J., T. Langer, …, F. U. Hartl. 1991. Chaperonin-mediated protein folding at the surface of groEL through a "molten globule"-like intermediate. *Nature.* 352:36–42.

61. Badcoe, I. G., C. J. Smith, …, A. R. Clarke. 1991. Binding of a chaperonin to the folding intermediates of lactate dehydrogenase. *Biochemistry.* 30:9195–9200.

62. Tyagi, N. K., W. A. Fenton, and A. L. Horwich. 2009. GroEL/GroES cycling: ATP binds to an open ring before substrate protein favoring protein binding and production of the native state. *Proc. Natl. Acad. Sci. USA.* 106:20264–20269.

63. Clare, D. K., D. Vasishtan, …, H. R. Saibil. 2012. ATP-triggered conformational changes delineate substrate-binding and -folding mechanics of the GroEL chaperonin. *Cell.* 149:113–123.

64. Motojima, F., and M. Yoshida. 2010. Polypeptide in the chaperonin cage partly protrudes out and then folds inside or escapes outside. *EMBO J.* 29:4008–4019.

65. Libich, D. S., N. L. Fawzi, …, G. M. Clore. 2013. Probing the transient dark state of substrate binding to GroEL by relaxation-based solution NMR. *Proc. Natl. Acad. Sci. USA.* 110:11361–11366.

66. Orland, H., and D. Thirumalai. 1997. A kinetic model for the chaperonin assisted folding of proteins. *J. Phys. I France.* 7:553–560.

67. Thirumalai, D. 1994. Theoretical Perspectives on In Vitro and In Vivo Protein Folding. Plenum Press, New York.

68. Lipari, G., and A. Szabo. 1980. Effect of librational motion on fluorescence depolarization and nuclear magnetic resonance relaxation in macromolecules and membranes. *Biophys. J.* 30:489–506.

69. Reference deleted in proof.

70. Gopich, I. V., D. Nettels, …, A. Szabo. 2009. Protein dynamics from single-molecule fluorescence intensity correlation functions. *J. Chem. Phys.* 131:095102.

71. Henry, E., and J. Hofrichter. 1992. Singular value decomposition: application to analysis of experimental data. *Methods Enzymol.* 210:129–192.

72. Rosenbluth, M., and A. Rosenbluth. 1955. Monte Carlo calculation of the average extension of molecular chains. *J. Chem. Phys.* 23: 356–359.

73. Schuler, B., E. A. Lipman, …, W. A. Eaton. 2005. Polyproline and the "spectroscopic ruler" revisited with single-molecule fluorescence. *Proc. Natl. Acad. Sci. USA.* 102:2754–2759.